SYNTHESIS AND STUDY OF QUARTNARY TRANSITION METAL FERRITE NANOCOMPOSITE WITH REDUCED GRAPHENE OXIDE ($Cu_xMn_{1-2x}Ni_yFe_{2-y}O_4$/rGO) FOR HIGH PERFORMANCE ENERGY STORAGE APPLICATIONS

M. ALI[a,*], M. ASHFAQ[a], S. M. ZAFAR IQBAL[b], M. F. MALIK[b]
[a]*Department of Chemistry, The Islamia University Bahawalpur, 63120, Pakistan*
[b]*Depatment of Electrical Engineering, Khawaja Fareed University of Engineering and Information Technology, Rahim Yar Khan, Pakistan*

In recent explorations, supercapacitors have been developed as energy storage devices that show excellent characteristics compared to conventional storage devices. The ferrite materials can have several redox states with high permeability which are attractive attributes for electrode materials for supercapacitors. Ferrite-based electrodes in supercapacitors is affected by the poor conductivity and cyclic stability. The literature suggests that both the electrical conductivity and the surface area of the electrode is increased by addition of graphene in ferrites. This hybrid supercapacitors of graphene and ferrite composites in which fast-reversible redox reactions causes storage of electrical energy has got great interest as an electrode material for next-generation supercapacitor applications. Many researcher reported binary, ternary ferrites nanocomposites with reduced graphene oxide as supercapacitor electrodes materials. In the present work, synthesis and study of quaternary transition metals (QTM) ferrites having formula $Cu_xMn_{1-2x}Ni_yFe_{2-y}O_4$ are mixed with reduced graphene oxide (rGO) to prepare nanocomposites of $Cu_xMn_{1-2x}Ni_yFe_{2-y}O_4$/rGO, for application in supercapacitor. The rGO based nanocomposites of QTM ferrites are explored using X-ray diffraction (XRD) analysis for structural morphology and the cyclic voltammetry (CV) technique is used for the performance analysis of the electrochemical activity of the QTM ferrites. The results show the specific capacitance of $Cu_xMn_{1-2x}Ni_yFe_{2-y}O_4$/rGO Naocomposite (282 F g^{-1}) is highly improved by the addition of rGO (90 F g^{-1}) compared with $Cu_xMn_{1-2x}Ni_yFe_{2-y}O_4$ (32 Fg^{-1}). The synthesized QTM ferrites are also explored by Thermal Analysis (TGA, DTGA, DSC), Fourier Transform Infrared (FT-IR), Field Scanning Emission Electron Microscopy (FESEM), as well as Energy Dispersive Spectroscopy (EDS). The results are discussed which suggest that the rGO based nanocomposites of QTM ferrites have promising scope for supercapacitor applications.

(Received August 11, 2019; Accepted December 6, 2019)

Keywords: Quaternary transition metal ferrites, Reduced graphene oxide, Supercapacitor, Cyclic voltammetry of ferrites

1. Introduction

The continuous decay of fossil fuel reserves has highlighted the energy crises around the globe. The scientists and engineers are trying to develop the novel technologies and materials for cost-effective energy storage and conversion devices by means of electrochemical systems [1,2]. In recent explorations, supercapacitors have been developed as energy storage devices that show excellent characteristics compared to conventional storage devices [2-4]. The supercapacitors work as energy storage devices that have high capacitance, low resistance, high energy density, a long-life cycle with quick charge and discharge compared to conventional capacitors. Due to these attributes, the supercapacitors have a greater demand for pulsed power sources. Some supercapacitors have been developed having typical values of low energy density (~5Wh kg^{-1}) than batteries while others have a higher value of the power density (~10 kW kg^{-1}) [1,3,9-11]. The supercapacitors have two types of major classes such as pseudocapacitors and electrochemical double-layer capacitor (EDLC) or simply electric double layer (EDL) capacitor[5]. In case of conducting polymers or metal oxides mixed electrode materials, the pseudocapacitors are

*Corresponding author: muradali70@yahoo.com

processed by age upon cycling while EDL capacitors with porous carbon electrodes do not process by age upon cycling [3,8,13,21]. The literature suggests that carbon nanotubes mixed supercapacitors don't show good performance without adding a pseudocapacitive component [1]. The peculiar attributes of electrode materials both physicochemical and electrochemical largely affect the efficiency and performance of supercapacitors [13]. It is observed that supercapacitors are best alternative storage devises for uninterruptible power supplies compare with conventional batteries [1,12]. In the case of EDL electrodes, non-faradaic process appears between electrode and electrolyte interface as whereas in pseudocapacitor fast reversible faradaic reactions causes charge storage at the electrode[6]. The optimal discharge time of EDL electrodes is less than a minute due to lower energy density which limits its wide application.

Generally, the active electrode materials in pseudocapacitors consist of conducting polymers, and d-block metals oxides such as Fe_3O_4, RuO_2, and MnO_2 [8,24-30]. Some of them as RuO_2 have specific capacitance more than 600 Fg^{-1} which is very high in the aqueous solution but it is not a cost-effective solution for commercialization due to high cost of RuO_2[7]. In case of neutral aqueous electrolyte the specific capacitance of MnO_2 is ~150 Fg^{-1} with a voltage of <1V while below 0 V it has no oxidation states that restrict its application as an electrode material [1]. Improved electrochemical performance is observed with mixed metal oxides such as various combinations of Ni,Mn, Fe,Co & etc. The spinel ferrites have formula MFe_2O_4, (M = Mn, Co or Ni) which exhibit excellent electrical, optical and magnetic properties with different redox states [24-25]. In a similar fashion, the general formula of the Ferro-spinel structure is M^{2+} [Fe^{3+}] O^{2-} which have ionic distribution. The ferric ion Fe^{3+} occupy the octahedral position while metal ion M^{2+} occupies the tetrahedral site as shown outside the bracket in the formula. The symbol M^{2+} ions are the metals with +2 oxidation state, metal like Ni^{+2}, $Cu^{2+,}$ $Mn^{2+,}$ Zn^{2+}, Co^{2+}, etc [26].

In several reports, NiFe, CoFe and MnFe have shown cost-effective attributes which are also environmentally friendly such as high specific capacitance, well-defined redox states which are more suitable behavior for supercapacitors[14]. This breakthrough revealed that ferrite materials can have several redox states with high permeability which are attractive attributes for electrode materials of supercapacitors [26]. The performance of ferrite-based electrodes in supercapacitors is affected by the poor conductivity and cyclic stability. The literature suggests that both the surface area and the electrical conductivity of the electrode is increased by the addition of graphene in metal oxides. The electrode materials of hybrid supercapacitors consist of graphene mixed metal oxides composites in which fast-reversible redox reactions causes storage of electrical energy. In this phenomenon, the ion adsorption/desorption occurs at the electrode/electrolyte interface. The addition of graphene also causes immobilization of active species through faster electron transfer in supercapacitors and also improves the stability of the whole hybrid system. The use of graphene in ferrite composites causes improvement in properties both physical and chemical of electrode materials. The supercapacitors performance depends upon ferrite-based electrodes which have superb electrical conductivity, surface area, excellent mechanical strength, and electron mobility. The transition metal oxides work as spacers between graphene nanosheets in hybrid supercapacitors that also hinder the agglomeration of graphene layers.

The general formula of mixed QTM ferrites is $ABEFe_2O_4$, (where A, B, and E represents a composites of Cu, Mn or Ni) yet its application is under the search for supercapacitors. These inexpensive ferrite nanocomposites might be potential electrode materials for the next generation supercapacitors. In recent years, Ternary Transition Metals ferrites have been reported as a promising candidate for applications of supercapacitor electrodes [38].

In this experimental work, ultrasonication technique is successfully used to synthesize rGO based $Cu_xMn_{1-2x}Ni_yFe_{2-y}O_4$ nanocomposite materials for supercapacitor applications whose capacitive behavior has been explored through XRD analysis, Thermal analysis, FT-IR, FESEM, as well as by EDS. The CV technique is used to check the electrochemical performance of the QTM ferrites type electrode whose XRD analysis reveals that these ferrite $Cu_xMn_{1-2x}Ni_yFe_{2-y}O_4$ have a single-phase spinel structure.

2. Experimental

2.1. Materials

In this work, all the chemicals of analytical grade are used to synthesize the QTM ferrite ($Cu_xMn_{1-2x}Ni_yFe_{2-y}O_4$) nanoparticles, Reduced graphene oxide (rGO) and QTM ferrite Nanocomposites without any further purifications.

Chemicals	**Company Brand**
Copper Nitrate trihydrate, $Cu(NO_3)_2{\cdot}3H_2O$	Sigma-Aldrich, 98%
Mn (II) Acetate tetrahydrate, $Mn(CH_3CO_2)_2{\cdot}4H_2O$	Beijing Chemical Works, 98%
Ni (II) Nitrate hexahydrate, $Ni(NO_3)_2{\cdot}6H_2O$	BDH, England, 98%
Fe (III) nitrate nonahydrate, $Fe(NO_3)\ 9H_2O$	Merck, 98%
NaOH	BDH England 99%
deionized water	analytical grade
Natural graphite powder	Sigma Aldrich

2.2. Synthesis of QTM ferrite nanoparticles

QTM ferrite nanoparticles was synthesised by using facile Coprecipitation technique. Solutions of molarities [0.2M Fe $(NO_3)_3$, 0.1M Ni $(NO_3)_2$, 0.1M 0.1M Cu $(NO_3)_2$, 0.1M Mn $(CH_3COO)_2$] were prepared using deionized water. These prepared solutions were mixed in required stoichiometric ratio (100 ml each) with constant stirring at 65 ^{0}C to get a homogenous solution. Then freshly prepared 3M aqueous Sodium Hydroxide solution was added dropwise until the pH of the reaction mixtures became about 11-12. Resultant mixture was again stirred for 6 hours at room temperature and was left overnight. Then the resultant mixture was filtered using filter paper. Then the precipitates were washed many times with a mixture of deionised warm water and ethanol until the pH of the washing was reduced to ~7. Drying of precipitates were carried out in oven at 100 ^{0}C for 2 hours. Then precipitates were grinded after drying in oven these and then heated at 950 ^{0}C using Muffle Furnace.

2.3. Synthesis of Graphene Oxide (GO)

Modified Hummer's method was used to synthesized graphite oxide by using graphite powder[26]. Concentrated H_2SO_4 (75 cm^3), graphite powder (1.5 g) and sodium nitrate (1.5 g) were added in a beaker and the resulting dispersion was stirred for 15 minutes at room temperature. Then, the beaker was placed on an ice bath and $KMnO_4$ (9 g) was added gradually suspension under constant stirring. Then mixture was removed from the ice bath after further stirring of 30 minutes. Then mixture was further stirred for 48 hours at room temperature and until the brown slurry or thick paste was obtained. Then deionized water about 150 cm^3 was added to the slurry with stirring for 10 minutes. The warm water (450 cm^3) and Hydrogen Peroxide (30 cm^3) was added gradually in the slurry to terminate the reaction. The yellow suspension obtained was washed (3-4 times) using a mixture of aqueous solution of 6% sulfuric acid and 1% hydrogen peroxide. The yellow suspension then centrifuges at 5000 rpm and washed with distilled water several times and finally the dark brown colored suspension of graphite oxide was obtained.

2.4. Synthesis of reduced graphene oxide (rGO)

Dark brown colored GO suspension was reduced by Hydrazine and Ammonia solution to get Reduced graphene oxide (rGO) [27]. Appoximatly30 cm^3 (30mg) of GO suspension was dispersed in 450 cm^3 of distilled water in an ultra-sonication bath. The suspension will subject to

ultra-sonication for about 1 hour. As result a light brown colored, homogeneous dispersion of GO was obtained. Then 225 μL of hydrazine solution (35wt% in water) and 1500 μL of ammonia solution (28 wt% in water) were added to the homogeneous dispersion of GO for reduction and the beaker containing reaction mixture was placed in a paraffin oil bath. The reaction mixture was stirred and heated (~90 ^{0}C) for 2 hours. The resulting suspension was subjected to centrifugation to obtain a black colored stable reduced graphene oxide (rGO). Finally, rGO was dried at 110°C in a Vacuum oven for 3-4 hours.

2.5. Synthesis of $Cu_xMn_{1-2x}Ni_yFe_{2-y}O_4$/rGO nano composite

QTM ferrite nanocomposite with rGO was synthesized by ultra-sonication method. 80 mg of synthesized QTM ferrite nanoparticles and 10mg of reduced graphene oxide was dispersed in 100 ml distilled water; the resulting dispersion was subject to ultrasonication for about 2 hours to obtain a homogeneous suspension QTM ferrite nanocomposite with rGO. The resulting suspension was filtered, washed with distilled water and dried at 120 ^{o}C for 12 hours in a vacuum oven.

2.6. Characterization

(i) The structural morphology of the as-prepared samples was investigated by X-ray diffraction using CuKα radiations source (λ=1.5418 Å), by Philips X' Pert PRO 3040/60 diffractometer

(ii) The structural morphologies were also explored by field emission scanning electron microscopy (FE-SEM, JEOL JSM-7401F).

(iii) The as-prepared samples were also explored using FTIR spectra recorded by FTIR spectrometer (SHMADZU).

(iv) Thermal analyzer (SDT Q600 V8.2 Build 100) is used to explore TGA of the as-prepared samples.

(v) The electrochemical measurments were performed on GAMRY INTERFACE 1000 E potentiostat.

3.Results and discussions

3.1. XRD analysis

XRD patterns of as-prepared $Cu_xMn_{1-2x}Ni_yFe_{2-y}O_4$, rGO and $Cu_xMn_{1-2x}Ni_yFe_{2-y}O_4$/rGO are shown in Figure (1). Figure (1a) illustrate the diffraction peaks at 2θ = 18.59°, 30.29°, 35.59°, 43.01°, 53.84, 57.50° and 63.10°, that correspond to crystal indices of (100), (220), (311), (400), (422), (511) and (440), respectively. The indexed peaks in the XRD pattern deduced from the data card (JCPDS no. 22-1086) that suggest cubic spinel structure of the $Cu_xMn_{1-2x}Ni_yFe_{2-y}O_4$). Figure (1b) shows two characteristic peaks at 25.15° and 42.29° in the XRD pattern associated with rGO from the reflections of diffraction planes (002) and (100). The XRD pattern of $Cu_xMn_{1-2x}Ni_yFe_{2-y}O_4$/rGO composite matches well with that of $Cu_xMn_{1-2x}Ni_yFe_{2-y}O_4$, and the intensity of diffraction peak of $Cu_xMn_{1-2x}Ni_yFe_{2-y}O_4$/rGO composite decreases markedly, and results suggest that the $Cu_xMn_{1-2x}Ni_yFe_{2-y}O_4$ crystallites are affected upon attaching to the rGO layers[29]. Furthermore, no obvious diffraction peak attributed to rGO is observed in Figure (1c), indicating that rGO is completely covered by $Cu_xMn_{1-2x}Ni_yFe_{2-y}O_4$ particles.

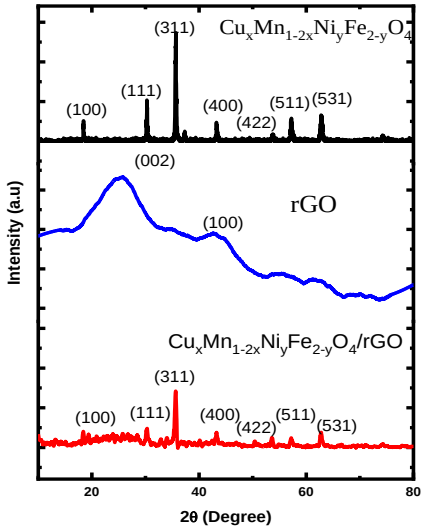

Fig. 1. Showing the XRD patterns (a) $Cu_xMn_{1-2x}Ni_yFe_{2-y}O_4$ Nanoparticles, (b) rGO and (c) $Cu_xMn_{1-2x}Ni_yFe_{2-y}O_4$/rGO Nanocomposite.

3.2. Analysis by FTIR spectroscopy

The spinel phase formation is confirmed by means of FTIR spectroscopy in the range 400–4000cm^{-1} of both the samples of $Cu_xMn_{1-2x}Ni_yFe_{2-y}O_4$ ferrites nanoparticles and $Cu_xMn_{1-2x}Ni_yFe_{2-y}O_4$/rGO. Two characteristic bands of spinel structure appear in the range of 400–600 cm^{-1}. Both octahedral and tetrahedral sub-lattice sites variations were differentiated because of the dissimilarity in the distance of ions. The highest band (υ_1) appears in the range of 500–600 cm^{-1} which belongs to the stretching vibrations of the metal at the tetrahedral site while the lowest band (υ_2) around 385–450 cm^{-1} belong to metal stretching at the octahedral site. These vibrational bands appear in a range of frequency i.e. 433, 486 and 567 cm^{-1} [30].

The results of FTIR spectroscopy revealed that absorption bands appear at the tetrahedral site in the frequency range 500–600 i.e. υ_1 associated of vibrations of metal-oxygen bond i.e. Fe-O while the absorption bands within the frequency range 400–475 cm^{-1} i.e. υ_2 belongs to the octahedral site and because of vibrations of metal-oxygen bond i.e. Mn-O.

The bending vibration of the moleculer bond H–O–H appears at 2341 cm^{-1} as absorption band of water molecules [31]. Whereas the peaks around 3400 cm^{-1}, 3495 cm$^{-1,}$ and 3475 cm^{-1} belong to the stretching vibrations of water molecules.

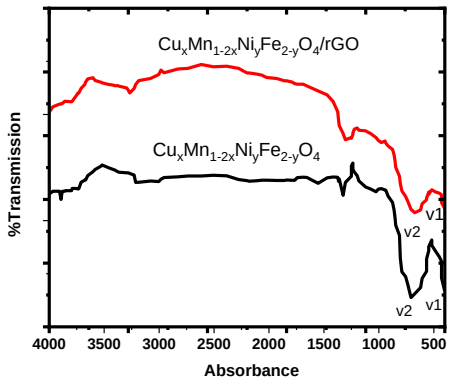

Fig. 2. Showing the FTIR patterns of $Cu_xMn_{1-2x}Ni_yFe_{2-y}O_4$ Nanoparticles (lower curve), and $Cu_xMn_{1-2x}Ni_yFe_{2-y}O_4$/rGO Nanocomposite (upper curve).

3.3. Morphological analysis

The structural morphology of the nanomaterials and nanocomposites mainly depends on the chemical compositions, the sizes, shapes, and distributions which were analyzed by SEM and EDX techniques. The chemical composition of the $Cu_xMn_{1-2x}Ni_yFe_{2-y}O_4$ and $Cu_xMn_{1-2x}Ni_yFe_{2-y}O_4$/rGO nanocomposites analyzed by the technique of energy dispersive spectroscopy (EDS). The EDS spectrum in Figure (3) shows the presence of C, O, Cu, Mn, Ni and Fe peaks. The results of EDS analysis are summarized in Table 1 in which exact compositions of the synthesized ferrite nanomaterial and $Cu_xMn_{1-2x}Ni_yFe_{2-y}O_4$/rGO nanocomposites are indicated, which confirm the purity of the nanomaterials. The SEM micrographs of a leaf-like a pattern belong to $Cu_xMn_{1-2x}Ni_yFe_{2-y}O_4$ as shown in Figure 4(a) which indicate that the synthesized spherical nanoparticles have uniform size distribution. The SEM micrographs are shown in Fig. 4(b) belong to $Cu_xMn_{1-2x}Ni_yFe_{2-y}O_4$/rGO nanocomposite have uniformly grown spherical nanoparticles on the graphene sheets.

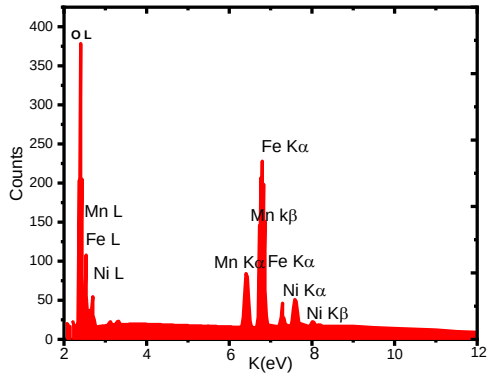

Fig. 3a. Showing the EDS spectrum of $Cu_xMn_{1-2x}Ni_yFe_{2-y}O_4$ Nanoparticles.

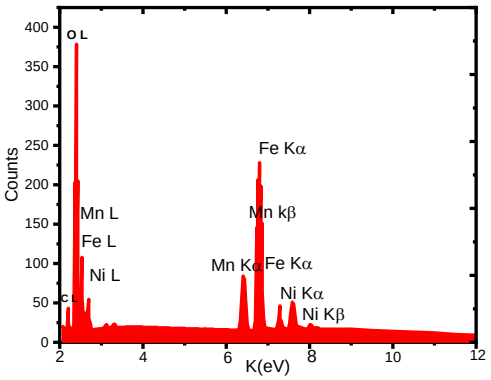

Fig. 3b. Showing the EDS spectrum of $Cu_xMn_{1-2x}Ni_yFe_{2-y}O_4$/rGO Nanocomposite.

Table 1. Showing the results of EDS analysis.

Sample	Copper wt %	Nickel wt %	Manganese wt %	Iron wt %	oxygen wt %	Carbon wt %
$Cu_xMn_{1-2x}Ni_yFe_{2-y}O_4$	7.01	13.21	13.27	34.32	31.50	-
$Cu_xMn_{1-2x}Ni_yFe_{2-y}O_4$/rGO	6.21	10.21	12.27	37.32	32.50	2.53

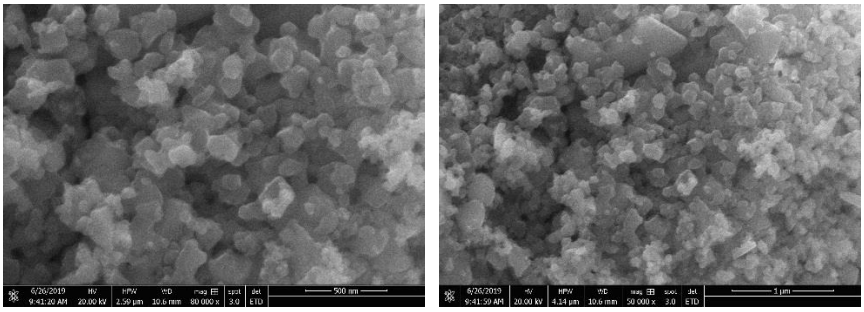

a) *b)*

Fig. 4. Showing the SEM images of the samples (a) $Cu_xMn_{1-2x}Ni_yFe_{2-y}O_4$ and of sample (b) $Cu_xMn_{1-2x}Ni_yFe_{2-y}O_4$/rGO.

3.4. Thermal analysis

In thermal decomposition or oxidation of samples, mass loss or gain is detected by the instrument which is used to explore the material characteristics. Thermal properties are explored by meas of three techniques (i) thermogravimetric analysis (TGA) (ii) differential thermal analysis (DTA) (iii) differential scanning calorimetry (DSC). Typical results of TGA, DTA, and DSC are discussed which were obtained by heating up the samples of $Cu_xMn_{1-2x}Ni_yFe_{2-y}O_4$ Nano-ferrite and of $Cu_xMn_{1-2x}Ni_yFe_{2-y}O_4$/rGO nanocomposite up to 1000℃.

The results TGA analysis are shown in Figure 5(a-c) which was performed using a heating rate of 10℃/min in air. Endothermic peaks accompanied by weight loss at 410-530℃ can be observed from the TGA curve of $Cu_xMn_{1-2x}Ni_yFe_{2-y}O_4$ nano-ferrite and of $Cu_xMn_{1-2x}Ni_yFe_{2-y}O_4$/rGO nanocomposite three weight loss regions were identified. Initial weight loss between room temperature to 100℃ appears due to evaporation of the residual water and absorbed by the samples during storage. The second weight loss at 410℃ to 530℃ temperature corresponds to the decomposition of iron oxide Fe_2O_3 and MnO_2 [32]. Finally, at a higher temperature, the TGA curve became more flattened, which indicate the formation of single-phase spinel structure.

DTA process was also carried out with a heating rate of 10℃/min in air and the results are shown in Figure 5(a-c). In the DTA curve, sharp peaks appeared at 477℃ and 489℃ for $Cu_xMn_{1-2x}Ni_yFe_{2-y}O_4$/rGO and $Cu_xMn_{1-2x}Ni_yFe_{2-y}O_4$ which indicates the exothermic nature of the reaction. Therefore, the weight loss at these temperatures is about 0.68%/ ^{0}C and 0.95% /^{0}C, respectively.

The DSC measurements are performed, to determine enthalpy changes for phase transitions. It is well clear from the above curves that a reduction in the mass percentage remains almost same/constant when the temperature is increased. Till 530℃ there is no major loss/reduction in mass and hence we can conclude that complete phase transformation has not attained till 530℃ or the material will have its phase formation only at a high temperature as mentioned earlier.

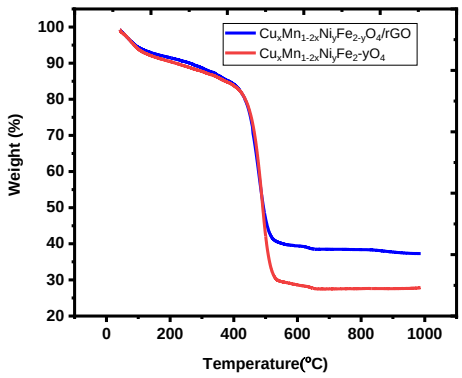

Fig. 5a. Showing the TGA of $Cu_xMn_{1-2x}Ni_yFe_{2-y}O_4$ and $Cu_xMn_{1-2x}Ni_yFe_{2-y}O_4$/rGO.

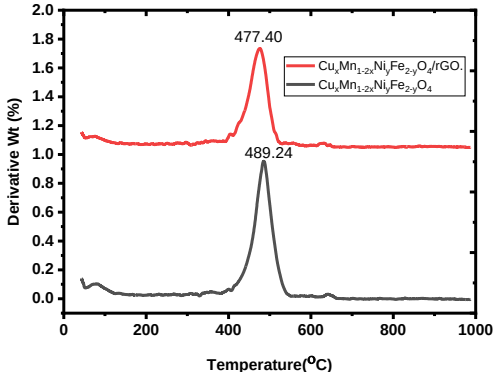

Fig. 5b. Showing the DTGA of $Cu_xMn_{1-2x}Ni_yFe_{2-y}O_4$ and $Cu_xMn_{1-2x}Ni_yFe_{2-y}O_4$/rGO.

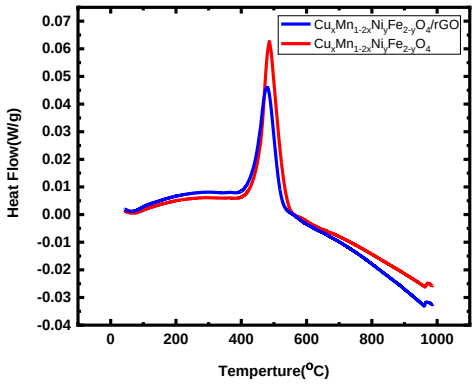

Fig. 5c. Showing the DSC of $Cu_xMn_{1-2x}Ni_yFe_{2-y}O_4$ and $Cu_xMn_{1-2x}Ni_yFe_{2-y}O_4$/rGO.

3.5. Electro-chemical analysis

The working electrode was prepared by depositing samples materials on FTO glass by drop casting method using nafion binder. 1M KOH solution was prepared. The setup of electrochemical analysis consists of the platinum reference electrode, silver/silver chloride electrode (standard) and the working electrode (materials were deposited on FTO glass). Three electrode system was connected to a potentiostat and dipped into a 1M KOH solution. Different scan cycles were performed at different sweep rates.

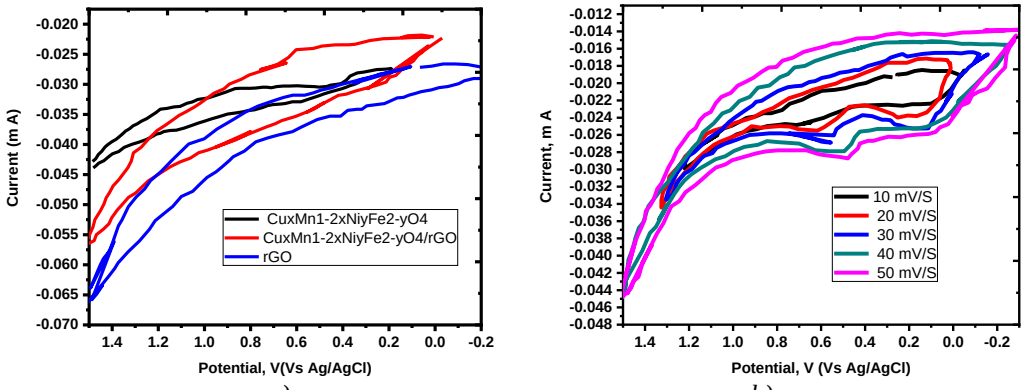

a) *b)*

Fig. 6. (a) Showing comparison CV curve at 100 mVs^{-1} of the samples (i) $Cu_xMn_{1-2x}Ni_yFe_{2-y}O_4$ (ii) $Cu_xMn_{1-2x}Ni_yFe_{2-y}O_4$/rGO (iii) rGO (b) CV curves of $Cu_xMn_{1-2x}Ni_yFe_{2-y}O_4$/rGO at different scan rates.

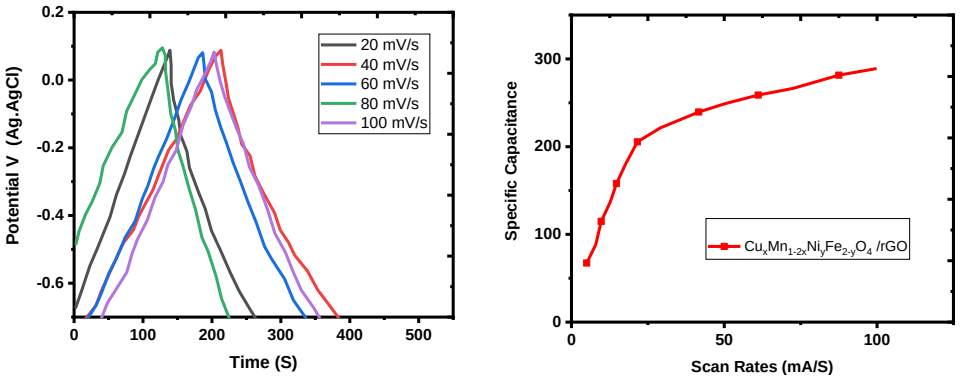

a) *b)*

Fig. 7. (a) Typical galvanostatic charge/discharge curves of $Cu_xMn_{1-2x}Ni_yFe_{2-y}O_4$/rGO (b) Variation of specific capacitance as a function of scan rate for the $Cu_xMn_{1-2x}Ni_yFe_{2-y}O_4$/rGO nanocomposite.

The CV technique is used to scrutinize the suitability of the prepared electrodes for supercapacitor application. The CV analysis was performed in the potential range of -0.02 to 1.5V vs Ag/AgCl in 1 M KOH electrolyte as shown in Figure 6(a,b).

The results show prominent redox peaks in the CV curve and also a deviation from the capacitive mechanism. The results show that the charge storage mechanism might be similar to battery type Faradaic reaction represented as Fe (II) → Fe (III).[35]

The area covered by the CV curve shows the amount of charge storage in the electrode. It was observed from the fig.(6a) that the area covered by $Cu_xMn_{1-2x}Ni_yFe_{2-y}O_4$/rGO electrode is more than $Cu_xMn_{1-2x}Ni_yFe_{2-y}O_4$ and rGO, which is attributed to the significant energy storage capability. Furthermore, the scan rate dependence of peak current at different scan rates in CV is shown in Figure 7(b) which dictates that peak current increases with increasing scan rates. In CV technique, the potential is with respect to a reference electrode so if the electrode resistance increases then it causes shifting of oxidation and reduction peaks towards positive and negative potential regions. Even at high scan rates, the $Cu_xMn_{1-2x}Ni_yFe_{2-y}O_4$/rGO nanocomposites show sharp redox peaks than the pristine $Cu_xMn_{1-2x}Ni_yFe_{2-y}O_4$ electrode which suggest good electrochemical reversibility at faster charge transfer. These results also suggest that the prepared electrodes are suitable for supercapacitor applications. The specific capacitance of the electrodes is estimated by the formula as given below:

$$Csp = \frac{\int Idv}{2\mu m \Delta V}$$

The symbols in the above equation represent the specific capacitance C_{sp}, the average current I(A), the mass of electrode material m(g) and the scan rate μ(mVS^{-1}). The specific capacitance value of composite electrode obtained at 10 mVs^{-1} is 282 Fg^{-1} which is highly improved compared with rGO (90 Fg^{-1}) and $Cu_xMn_{1-2x}Ni_yFe_{2-y}O_4$ (32 Fg^{-1}). The cause of the greatly enhanced specific capacitance is the synergistic effect between rGO and $Cu_xMn_{1-2x}Ni_yFe_{2-y}O_4$. It also attributed due to the unique structure of $Cu_xMn_{1-2x}Ni_yFe_{2-y}O_4$/rGO composite, which effectively improves the interconnection of active materials that is between QTM Ferrite nanoparticals and rGO and enhanced Capacitance of the nanocomposite..

Shown in Fig. (7a) are the charge/discharge curves is the cycling stability curve of $Cu_xMn_{1-2x}Ni_yFe_{2-y}O_4$/rGO nanocomposites electrode. It is observed that the charge/discharge behavior is almost steady within the voltage window –1.0 to 1.0 V after many cycles. So it can be conculuded that th composite could retain 80% of its initial capacitance after many repetitive cycle, indicating $Cu_xMn_{1-2x}Ni_yFe_{2-y}O_4$/rGO composite might be a potential candidate as an electrode-materials for supercapacitor. The shape of CV curve as shown in fig.(6b) maintains its

initial shape without any variation which suggests cycling stability is excellent that inhibits the capacitance loss and gain during repetitive cycles

4. Conclusions

In this work, modified simple chemical methods with superior electrochemical properties and Hummer's method is successfully used to synthesize the $Cu_xMn_{1-2x}Ni_yFe_{2-y}O_4$/rGO nanocomposites. The structural morphology of the prepared $Cu_xMn_{1-2x}Ni_yFe_{2-y}O_4$/rGO nanocomposites was confirmed by the XRD, FESEM- EDS, FTIR spectroscopy. The thermal analysis studies shows stability of synthesised materials at high tempertaures. The Cyclic voltammetry experiments prove that synthesized nanocomposites have stable maximum discharge capacity which is higher specific capacitance value (282 Fg^{-1}) compared to $Cu_xMn_{1-2x}Ni_yFe_{2-y}O_4$ electrode materials. Moreover, the rate capability and cyclic stability of $Cu_xMn_{1-2x}Ni_yFe_{2-y}O_4$/rGO nanocomposite are superior to $Cu_xMn_{1-2x}Ni_yFe_{2-y}O_4$ nanoparticles. These results suggest that $Cu_xMn_{1-2x}Ni_yFe_{2-y}O_4$/rGO nanocomposites have fascinating electrochemical activity. These nanocomposites might be a potential candidate as electrode material for high performance of supercapacitors or in the next-generation energy storage devices.

Acknowledgments

The authors would like to thank the Ministry of Higher Education Commission of Pakistan to provide support for research activities at IUB Baghdad Road Bahawalpur.

References

[1] P. Simon, Y. Gogotsi, Materials for Electrochemical Capacitors. Nat. Mater. **7**(11), 845 (2008).
[2] S. Zhang, N. Pan, Supercapacitors Performance Evaluation. Adv. Energy Mater. **5**(6), 1401401 (2015).
[3] B. Bashir, W. Shaheen, M. Asghar, M. F. Warsi, M. A. Khan, S. Haider, I. Shakir, M. Shahid, J. Alloys Compd. **695**, 881 (2017).
[4] W. Zhou, J. Liu, T. Chen, K. S. Tan, X. Jia, Z. Luo, C. Cong, H. Yang, C. M. Li, T. Yu, Phys. Chem. Chem. Phys. **13**(32), 14462 (2011).
[5] M. D. Stoller, S. Park, Y. Zhu, J. An, R. S. Ruoff, Nano Lett. **8**(10), 3498 (2008).
[6] T. Y. Kim, H. W. Lee, M. Stoller, D. R. Dreyer, C. W. Bielawski, R. S. Ruoff, K. S. Suh, ACS Nano **5**(1), 436 (2011).
[7] W. Zhang, B. Quan, C. Lee, S. K. Park, X. Li, E. Choi, G. Diao, Y. Piao, ACS Appl. Mater. Interfaces **7**(4), 2404 (2015).
[8] Z. Wang, X. Zhang, Y. Li, Z. Liu, Z. Hao, J. Mater. Chem. A **1**(21), 6393 (2013).
[9] B. E. Conway, Electrochemical Supercapacitors: Scientific Fundamentals and Technological Applications, 1st ed; Kluwer Academic/Plenum Publishers: New York, (1999).
[10] Y. Q. Zhao, M. Lu, P. Y. Tao, Y. J. Zhang, X. T. Gong, Z. Yang, G. Q. Zhang, H. L. Li, J. Power Sources **307**, 391 (2016).
[11] X. Cui, R. Lv, R. U. R. Sagar, C. Liu, Z. Zhang, Electrochim. Acta **169**, 342 (2015).
[12] S. Maiti, A. Pramanik, S. Mahanty, Chem. Commun. **50** (79), 11717 (2014).
[13] E. Umeshbabu, G. Rajeshkhanna, G. R. Rao, J. Solid State Electrochem. **20**(7), 1837 (2016).
[14] L. Li, H. Bi, S. Gai, F. He, P. Gao, Y. Dai, X. Zhang, D. Yang, M. Zhang, P. Yang, Sci. Rep. **7**, 43116 (2017).
[15] L. Jiang, Z. Fan, Nanoscale **6** (4), 1922 (2014).
[16] S. Han, D. Wu, S. Li, F. Zhang, X. Feng, Adv. Mater. **26**(6), 849 (2014).
[17] X. Fan, B. D. Phebus, L. Li, S. Chen, Sci. Adv. Mater. **7**(10), 1916 (2015).
[18] Q. Ke, J. Wang, J. Materiomics **2**(1), 37 (2016).

[19] M. Winter, R. J. Brodd, Chem. Rev. **104**(10), 4245 (2004).
[20] W. Chee, H. Lim, Z. Zainal, N. Huang, I. Harrison, Y. Andou, J. Phys. Chem. C **120**(8), 4153 (2016).
[21] L. L. Zhang, X. Zhao, Chem. Soc. Rev. **38**(9), 2520 (2009).
[22] L. Ma, X. Shen, H. Zhou, Z. Ji, K. Chen, G. Zhu, Chem. Eng. J. **262**, 980 (2015).
[23] C. Liu, Z. Yu, D. Neff, A. Zhamu, B. Z. Jang, Nano Lett. **10**(12), 4863 (2010).
[24] H. Jiang et al., Chem Communication **48**(20),2606 (2012).
[25] M.-T. Lee et al., J Power Sources **185**(2),1550 (2008)
[26] S.-K. Chang et al., Electrochim Acta **67**(67), (2012).
[27] S. Sun et al., J Am Chem Soc **126**(1), 273 (2004).
[28] C. D. Lokhande, D. P. Dubal, O.-S. Joo, Curr Appl Phys. **11**(3), 255 (2011).
[29] J. L. Gunjakar et al., Appl Surf Sci. **254**(18), 5844 (2008).
[30] D. Ravinder, A. V. Ramana Reddy, Mater Lett. **38**(4), 265 (1999).
[31] L. Zheng, C. Wang, Y. Dong, H. Bian, T. F. Hung, J. Lu, Y. Y. Li, Appl. Surf. Sci. **362**, 399 (2016).
[32] Y. Zheng, Z. Li, J. Xu, T. Wang, X. Liu, X. Duan, Y. Ma, Y. Zhou, C. Pei, Nano Energy **20**, 94 (2016).
[33] K. Wasinski, M. Walkowiak, P. Połrolniczak, G. Lota, J. Power Sources **293**, 42 (2015).
[34] S. Marappan, H. Itaru, Graphene and Graphene-based Nanocomposites for Electrochemical Energy Storage, in: Nanotechnology in Advanced Electrochemical Power Sources, Pan Stanford, 221 (2014).
[35] Y. Bai, R. B. Rakhi, W. Chen, H. N. Alshareef, J. Power Sources **233**, 313 (2013).
[36] D. Li, M. B. Muller, S. Gilje, R. B. Kaner, G. G. Wallace, Nat. Nano **3**, 101(2008).
[37] A.S. Faheim, M.K. Abd El Fattah, A.H. Abdul Rahman, A. J. Badawi. Nanomater, (2014).
[38] Bhamini Bhujun Michelle T.T. Tan, Anandan S. Shanmugam, Study of mixed ternary transition metal ferrites as potential electrodes for supercapacitor applications, http://dx.doi.org/10.1016/j.rinp.2016.04.010